Title: BODIPY-Based Photothermal Agents with Unprecedented Phototoxic Indices for Cancer Treatment

Authors:

Lukas Schneider,[‡1] Martina Kalt,[‡,§,1,2] Samuel Koch,[1] Shanmugi Sithamparanathan,[1] Veronika Villiger,[1] Johann Mattiat,[1] Flavia Kradolfer,[1] Ekaterina Slyshkina,[1] Sandra Luber,[1] Mathias Bonmarin,[3] Caroline Maake,[2] and Bernhard Spingler[*1]

[‡] These authors contributed equally to the work.

[*] To whom correspondence should be addressed. E-mail: spingler@chem.uzh.ch

Affiliations:

[1] Department of Chemistry, University of Zurich, CH-8057 Zurich, Switzerland.

[2] Institute of Anatomy, University of Zurich, CH-8057 Zurich, Switzerland.

[3] School of Engineering, Zurich University of Applied Sciences, CH-8400 Winterthur, Switzerland.

[§] Current affiliation: EAWAG, CH-8600 Dübendorf, Switzerland

Abstract:

Here we report six novel, easily accessible BODIPY-based agents for cancer treatment. In contrast to established photodynamic therapy (PDT) agents, these BODIPY-based compounds show additional photothermal activity and their cytotoxicity is not dependent on the generation of reactive oxygen species (ROS). The agents show high photocytotoxicity upon irradiation with light and low dark toxicity in different cancer cell lines in 2D culture as well as in 3D multicellular tumour spheroids (MCTSs). The ratio of dark to light toxicity (phototoxic index, PI) of these agents reaches striking values exceeding 830'000 after irradiation with energetically low doses of light at 630 nm. The oxygen-dependent mechanism of action (MOA) of established photosensitizers (PSs) hampers effective clinical deployment of these agents. Under hypoxic conditions (0.2% O_2), which are known to limit the efficiency of conventional PSs in solid tumours, photocytotoxicity was induced at the same concentration levels, indicating an oxygen-independent photothermal MOA. With a PI exceeding 360'000 under hypoxic conditions, both PI values are the highest reported to date. We anticipate that

small molecule agents with a photothermal MOA, such as the BODIPY-based compounds reported in this work, may overcome this barrier and provide a new avenue to cancer therapy.

Keywords:

Medicinal Chemistry, Photodynamic Therapy, Photothermal Therapy, Phototherapy, Cancer

Introduction:

In the last couple of decades, photodynamic therapy (PDT) has become a widely used therapeutic method for the treatment of a variety of premalignant and malignant diseases.[1-3] PDT conventionally involves the application of a photosensitizer (PS) that is activated by light in the tissue to be treated. This method has many potential applications due to the advantages it presents as a non- or minimally invasive therapeutic. PDT does not exhibit cumulative toxicity and its activation can be controlled both spatially and temporally. The adjustable light used, as well as the short diffusion radius of the emerging reactive oxygen species (ROS), minimize the damage to surrounding healthy tissue.[4-5]

The mechanism of action (MOA) consists of the PS-mediated generation of ROS from its first excited triplet state.[6] The generated ROS involves singlet oxygen ($^1O_2$) via the type II mechanism, or radical species such as hydroxyl radicals ($OH^{\bullet}$) and superoxide anions ($O_2^{\bullet-}$) via the type I mechanism.[7] Both mechanisms depend on molecular oxygen ($^3O_2$) in the tissue, leading to reported clinical resistance under hypoxia. This MOA is a major drawback as solid tumours are invariably less well-oxygenated than non-malignant tissue.[8-12]

Alternative MOAs to the type I and type II pathways have been reported in literature despite a lack of consensus regarding the definition of oxygen-independent mechanisms.[10, 13] A modified type I mechanism, called type III, has been described based on an interaction between the PS in its first excited triplet state and doublet free radicals with diffusion-controlled rate constants.[14-19] Other reports of oxygen-independent mechanisms involve the generation of toxic photoproducts from upper excited triplet states,[20] photoinduced electron-transfers leading to cycloaddition reactions,[21-22] and structural changes upon excitation that allow binding to intracellular targets.[10, 18] These properties currently preclude therapeutic deployment. Additional agents for phototherapy undergoing photoredox catalysis have been reported recently.[23-24]

Furthermore, phototherapeutic treatment methods have emerged based on photothermal therapy (PTT). PTT applies functional biomedical and bioactive nanomaterials activated by light in the near-infrared (NIR) range to eliminate tumour cells via the generation of heat upon irradiation.[25-28] Despite the many advantages of PTT, drawbacks concerning biocompatibility, biodegradation, long-term toxicity, and threats of these nanomaterials to the environment remain unresolved.[25] Small molecules rather than

nanomaterials have been employed for PTT, however all the previous approaches required a nanoprecipitation step, again precluding straightforward use in a biological context.[29-31]

Here, we report six novel metal-free BODIPY-based (boron-dipyrromethene) agents that are able to undergo an oxygen-independent photothermal MOA upon excitation with small doses of light in the visible range. The compounds are easily accessible and have phototoxic indices (PIs), the ratio of dark to light toxicity,[32-34] of over 830'000 in cancer cells under normoxic conditions and over 360'000 under hypoxic conditions (0.2% O_2). BODIPY-based compounds have favourable properties, being easily accessible small molecules that are excitable with tissue-penetrating red light at 630 nm. In contrast to conventional PTT systems, they can be applied in solution and do not require additional additives or the nanoprecipitation step prior to application. We anticipate that their toxicity to cancer cells through local light-to-heat conversion might help to overcome the enormous drawback of hypoxia resistance in PDT as well as the toxicity issues of nanomaterials in PTT.

Results:

Characterization:

All compounds are based on an asymmetric BODIPY-based structure[35] with an extended π-system and varying bathochromically-shifting moieties. BODIPYs are known for their high chemical stability and molar extinction coefficients, and their photophysical properties as well as their solubility can be fine-tuned by countless possibilities of synthetic functionalization.[36] Therefore, they are promising candidates for light-induced cancer therapy. Compounds **1a**, **2a**, and **3a** (**Fig. 1a**) were synthesized according to the synthetic pathway shown below (**Fig. 1b**); their syntheses are described in detail in the supporting information (**S1 – S5**). Compounds **1b**, **2b**, and **3b** (**Fig. 1a**) were obtained after mono-iodination of compounds **1a**, **2a**, and **3a**, respectively, and contain an additional iodine atom to induce a heavy-atom effect and higher triplet state quantum yields.[37-38] All compounds were characterized as described in the supporting information (**S1 – S5**) by spectroscopic and analytical data including UV-Vis, fluorescence emission, IR, NMR, and mass spectroscopy, liquid chromatography, single crystal X-ray analysis (**S1 – S6**, **Fig. S1**), elemental analysis, as well as partition constant determination (**S7**, **Tab. S1**).

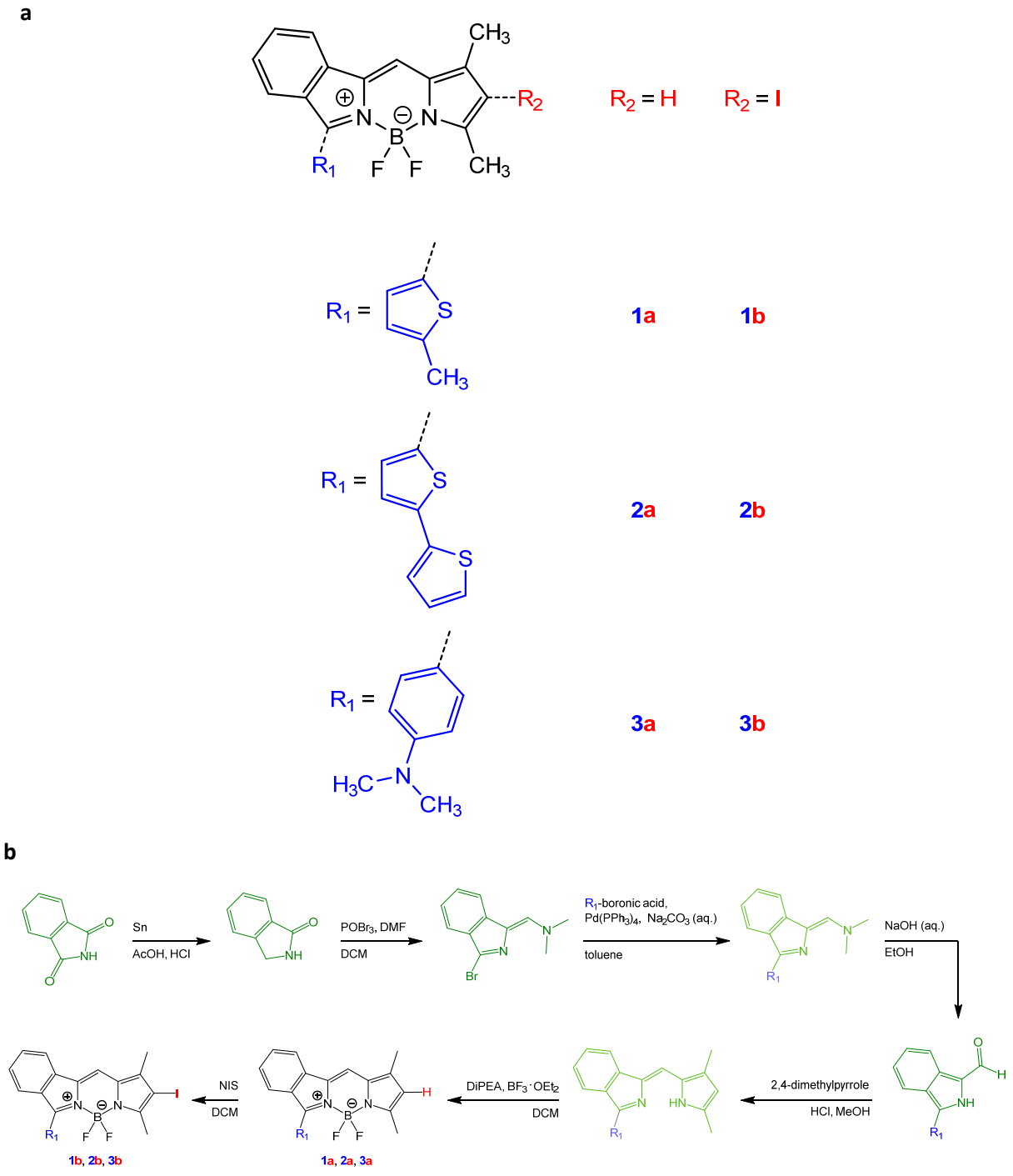

Fig. 1: **a**, Chemical structures of **1a** - **3a**, as well as **1b** - **3b**, the corresponding crystal structures are shown in the supporting information (**Fig. S1**). **b**, The synthetic pathway towards the common precursor compounds (shown in green) as well as BODIPYs **1a**, **1b**, **2a**, **2b**, **3a**, and **3b** (shown in black). The detailed experimental procedures are reported in the supporting information (**S1** – **S5**). Intermediates shown in light green were not isolated. R_1 (shown in blue) stands for the corresponding residue group shown in part **a** of this figure.

Photophysical measurements were carried out for all six compounds. The singlet oxygen quantum yields

(Φ_Δ) (**Tab. 1**, **Tab. S2**) of **1a**, **1b**, **2a**, **2b**, **3a**, and **3b** were determined by applying light at a wavelength of 630 nm (**Fig. S3**) based on a direct method (**S9**).[36, 39-42] Fluorescence quantum yields (Φ_F) (**Tab. 1**, **Tab. S3**) of **1a**, **1b**, **2a**, **2b**, **3a**, and **3b** were determined as described in **S10**. All compounds are highly fluorescent in aprotic solvents like DCM and toluene, and non-fluorescent in H_2O, and all compounds except **3a** and **3b** are highly-fluorescent in the protic solvent MeOH with Φ_F values ranging from 0.33 to 0.82, while the protic character of MeOH quenches the fluorescence emission of **3a** and **3b** to $\Phi_F \leq$ 0.03. The fluorescence lifetimes (τ_F) (**Tab. 1**, **Tab. S4**) of all compounds have been determined in MeOH (**S11**), resulting in τ_F values in the range of 3.22 to 13.6 ns. The absorption maximum of all studied compounds is in the range between 588 and 617 nm in MeOH and the fluorescence emission maximum between 620 and 655 nm. In MeOH, DCM and toluene all compounds exhibit a rather sharp absorption maximum, while in H_2O the absorption peak is very broad with distinctly lower extinction coefficients compared to the other solvents. The addition of the iodine atom to the pyrrolic position bathochromically shifts the absorption maximum between 8 nm and 15 nm compared to the non-iodinated analogue compound. The compound pair **2a** and **2b** exhibit their absorption maximum at the longest wavelengths due to the presence of a second thiophene unit that is contributing to the photochemical system of the compounds. Non-iodinated compounds **1a**, **2a**, and **3a** do not generate $^1O_2$, while the iodine-containing derivatives **1b** and **2b** show a low Φ_Δ of 0.26 ± 0.05 and 0.15 ± 0.01, respectively, in contrast to **3b** that does not generate $^1O_2$ at all in MeOH-d_4. BODIPY-based compounds containing a *N*,*N*-dimethylaniline moiety like of **3b** are known for undergoing intramolecular charge transfers (ICTs) in the non-protonated state upon irradiation that quenches the $^1O_2$ generation.[36, 43-45] This correlates with the triplet state lifetimes (τ_T) (**Tab. 1**, **Tab. S5**) determined as described in **S12**. While a τ_T of 120 ns was measured for **1b**, and a τ_T of 147 ns for **2b**, no triplet state was detected for the third compound of the iodinated series, **3b**. No triplet state could be detected in the case of all non-iodinated compounds **1a**, **2a,** and **3a**, which is also in line with the observed Φ_Δ values. The ability to generate $^1O_2$ (type II mechanism) and the ability to generate hydroxyl radicals ($^\bullet$OH), superoxide anions ($O_2^{\bullet-}$) and/or other ROS (type I mechanism) was investigated with the corresponding chemical sensors[46] as described in **S13** (graphs shown in **Fig. S9**). Compared to the standard methylene blue (**MB**), only small amounts of ROS were detected in the case of **1a**, **1b**, **2a**, **2b**, **3a**, and **3b** after irradiation with light at 630 nm (**Fig. S8**) for 40 min (total applied energy = 5.0 J/cm^2). This suggests that the generation of ROS is not the primary mechanism to induce photocytotoxicity.

The first two excited singlet (S_x) and triplet (T_x) states of **1a**, **1b**, **2a**, **2b**, **3a**, and **3b** were calculated at TDDFT level using geometry optimized structures (**S14**). The BLYP exchange-correlation functional[47-48] was employed for the geometry optimizations and the TDDFT calculations. Additionally, TDDFT calculations were carried out using the B3LYP hybrid exchange-correlation functional[48-50] (results shown in **Tab. S6**). Visualizations of the calculated natural transition orbitals (NTOs)[51] for the first singlet state (**S15**) provide an intuitive particle-hole picture after the immediate absorption (results shown in **Fig. S10**). The results indicate that the long-lived first excited triplet state (T_1) is energetically

accessible for all six compounds. As the calculations were carried out for optimized ground state structures the calculated energies correspond to vertical excitation energies. In order to obtain insight into the actual photochemical processes involved non-adiabatic dynamics would be required the computational cost of which goes beyond the scope of this work. Additional calculations performed using the COSMO solvation model[52] to account for solvation effects indicated comparable results (results shown in **Tab. S7**).

The photostability of all compounds was determined (**S16**) by measuring the photobleaching quantum yields (Φ_d) (**Tab. 1**, **Tab. S8**). Compounds **1a**, **3a**, and **3b** were photostable under the applied conditions in DMF, while **1b**, **2a**, and **2b** showed small Φ_d in comparison to zinc phthalocyanine (**ZnPc**) (Φ_d = 0.23×10^{-4} in DMF[53]).

Compound	Absorption λ_{max} (nm), log(ε)	Emission λ_{max} (nm)	Φ_Δ	Φ_F	τ_F (ns)[a]	τ_T (ns)[a]	Φ_d
1a	590, 4.69	620	0	0.82 ± 0.06	13.6	-	Photostable (> 2 h)
1b	598, 4.70	633	0.26 ± 0.05	0.50 ± 0.03	4.69	120	$(6.5 \pm 0.6) \times 10^{-6}$
2a	607, 4.69	651	0	0.43 ± 0.01	5.40	-	$(7.8 \pm 0.5) \times 10^{-5}$
2b	617, 4.65	655	0.15 ± 0.01	0.33 ± 0.04	3.45	147	$(6.4 \pm 0.3) \times 10^{-6}$
3a	588, 4.65	627	0	0.025 ± 0.001	3.72	-	Photostable (> 2 h)
3b	597, 4.55	638	0	0.010 ± 0.001	3.22	-	Photostable (> 2 h)

Tab. 1: Photophysical properties of **1a**, **1b**, **2a**, **2b**, **3a**, and **3b**. UV-Vis absorption measured in MeOH; Fluorescence emission measured in MeOH; Φ_Δ measured in MeOH-d_4; Φ_F measured in MeOH; τ_F measured in MeOH; τ_T measured in MeOH; Φ_d measured in DMF. Additional UV-Vis absorption, and fluorescence emission spectra and data measured in H_2O, MeOH, DCM and toluene are reported in the supporting information. [a] The estimated errors for the values reported are 10%.

Photocytotoxicity:

The photocytotoxicity of **1a**, **1b**, **2a**, **2b**, **3a**, and **3b** (**Tab. 2**, **Fig. S11**) was studied as described in **S17-**

S19, the light dose dependency (**Fig. S14**) and time-dependent cellular uptake (**Fig. S15)** were determined as described in **S20-S21**. HeLa human cervical cancer cells were either treated with the compounds or without compounds as treatment control, and further and irradiated with light of 630 nm (**Fig. S8**) for 40 min corresponding to an energy dose of 5.0 J/cm^2. Despite the high Φ_F values, low Φ_Δ values and low levels of generated ROS, **1a**, **1b**, **2a**, **2b**, **3a**, and **3b** showed high photocytotoxicity when exposed to this low total energy dose. The IC_{50} (half maximal inhibitory concentration) values of all iodinated compounds are in the one- or two-digit nanomolar range. As expected, they are distinctly lower than for all non-iodinated compounds. The presence of a T_1 state, based on the measurable τ_T, does not correlate with the observed photocytotoxicities, and the non-iodinated compounds **1a**, **2a,** and **3a** as well as the iodinated compound **3b** show photocytotoxicity. All compounds furthermore show very low toxicity in the dark with IC_{50} values up to > 5 mM. The most interesting non-iodinated/iodinated compound pair **1a** and **1b** is non-toxic in the dark in HeLa cells (IC_{50} > 5 mM), while **1a** as the non-iodinated compound has an IC_{50} value of 0.730 ± 0.004 μM upon irradiation and **1b** as the iodinated compound has an IC_{50} value of 0.0060 ± 0.0003 μM upon irradiation. This is equal to a PI of over 830'000 for **1b**. This is, to the best of our knowledge, the highest PI value reported for any photosensitizer. Photocytotoxicity determinations of **1a** and **1b** in other cell lines such as in the A2780 human ovarian cancer cell line (**Tab. S9**, **Fig. S12**), and MRC-5 human fetal lung fibroblast cell line (**Tab. S10**, **Fig. S13**) showed similar photochemical and phototoxic properties.

Compound	IC_{50} (irradiation, μM)	IC_{50} (dark, μM)	PI
1a	0.730 ± 0.004	> 5000	> 6800
1b	0.0060 ± 0.0003	> 5000	> 830’000
2a	0.130 ± 0.003	1250 ± 88	9600
2b	0.0350 ± 0.0009	2070 ± 269	59’000
3a	0.56 ± 0.04	1330 ± 123	2400
3b	0.032 ± 0.002	2160 ± 139	68’000

Tab. 2: IC_{50} values of **1a**, **1b**, **2a**, **2b**, **3a**, and **3b** in the dark and upon irradiation, and the corresponding PI values. Compound **1b** is the most efficient compound with an IC_{50} value of 0.0060 ± 0.0003 μM upon light irradiation, > 5000 μM in the dark and a PI of > 830'000.

Photocytotoxicity and growth-inhibiting properties (**Fig. 2**, **Tab. S11**, **Fig. S16**) of the most promising compound **1b** in HeLa 3D multicellular tumour spheroids (MCTSs), which are known to simulate the conditions found in clinically treated tumors[54-55], have been determined as described in **S22-S24**. The photocytotoxicity assay with **1b** was carried out under analogous conditions to those used for determining photocytotoxicity in HeLa cell monolayers using light with a wavelength of 630 nm (**Fig. S8**) and an irradiation time of 40 min corresponding to an energy dose of 5.0 J/cm^2. IC_{50} values for **1b**

in HeLa MCTSs have been determined to be 0.12 ± 0.04 μM after light exposure and > 1660 μM in the dark, resulting in a PI of > 13'800. This underlines the photocytotoxic potency of **1b** observed in the different cell lines in a simple model system with tumour-like conditions.

The growth-inhibiting properties of **1b** in HeLa MCTSs were measured before and after treatment with **1b**. MCTSs treated with **1b** and irradiated with light were compared to three control conditions: MCTSs treated with **1b** and kept in the dark, MCTSs treated with the solvent vector only and kept in the dark, and MCTSs treated with the solvent vector upon irradiation with light. All three control conditions led to linear MCTS growth during the observation window with an average MCTS size of 181% on day five compared to the initial size. MCTSs treated with **1b** and subsequent irradiation with light of 630 nm started dissolving on day three visible in the inflation of the MCTSs to 233% of the initial size followed by a steady decrease in size. This shows that **1b** is not just decreasing the growth rate of the MCTSs like cisplatin[42], but actively destroying them upon irradiation. The observed change in size of the MCTSs is shown in micrographs of single MCTSs over time (**Fig 2a**), as well as MCTS size relative to time (**Fig 2b**).

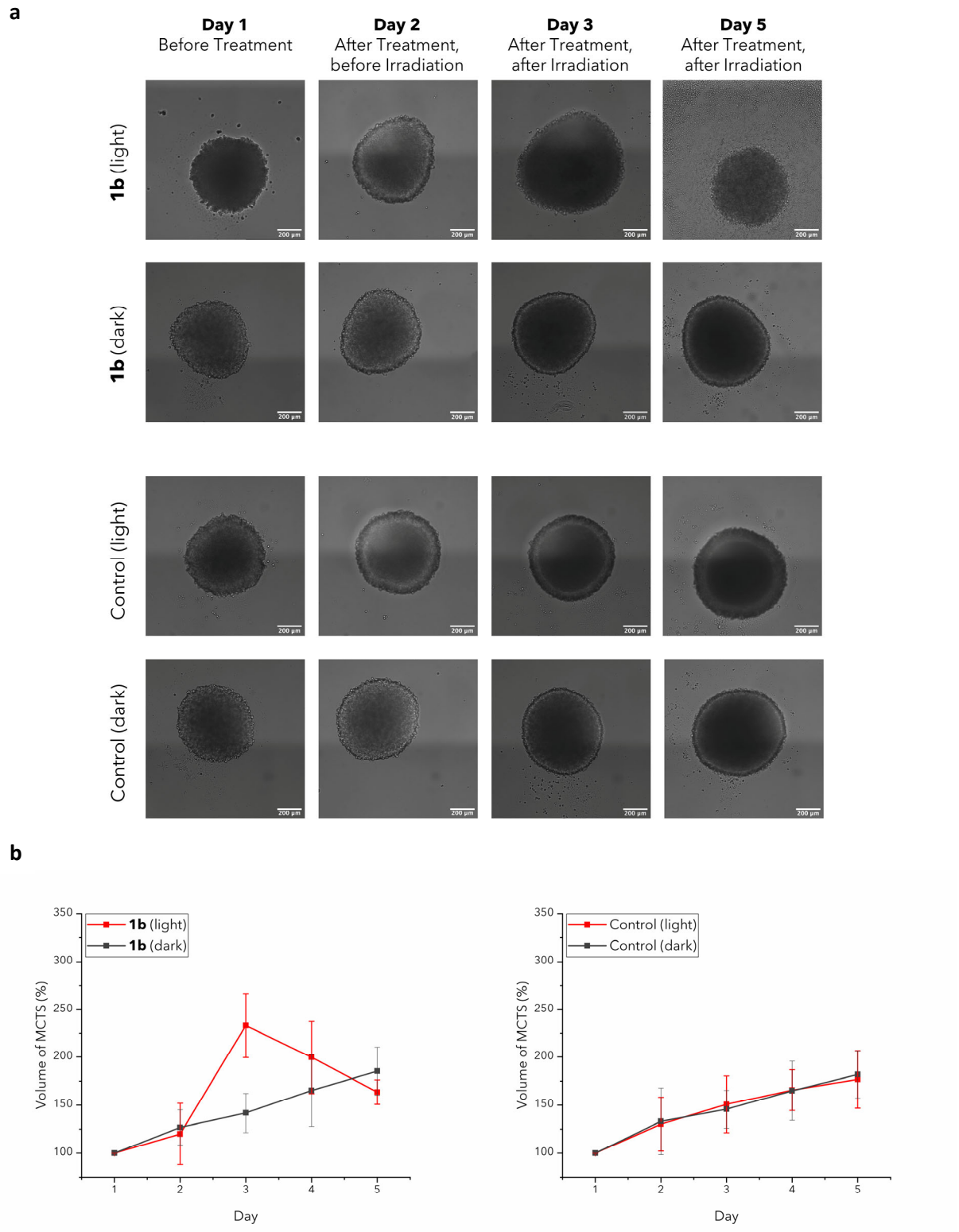

Fig. 2: **a**, Micrographs of 3D HeLa multicellular tumor spheroids (MCTSs) taken over five days (scale bars = 200 µm). **b**, Monitored growth of 3D HeLa MCTSs over five days compared to the initial size. MCTSs were treated either with **1b**, or the solvent vector (Control), and irradiated either with light of 630 nm (light), or kept in the dark (dark).

Because MCTSs also simulate tumour hypoxia and proliferation gradients to the centre[54-55], the observed

effectivity in HeLa MCTSs indicated a possible efficiency under hypoxic conditions. To test this hypothesis, the photocytotoxicity determination for compounds **1a** and **1b** in monolayer HeLa cells was repeated under hypoxic conditions (**Tab. 3**, **Fig. S17**) as described in **S25**. Both **1a** and **1b** proved to be highly effective in HeLa cells under hypoxic conditions while being treated and excited analogous to conditions used to test phototoxicity in HeLa cells under normoxic conditions. IC_{50} values in the dark were, as expected, slightly lower under hypoxic conditions with values > 2500 µM for both **1a** and **1b**. While the IC_{50} value upon excitation with light of the non-iodinated compound **1a** increased to 1.87 ± 0.08 µM, the IC_{50} value of the iodinated compound **1b** remained virtually unchanged with a value of 0.0069 ± 0.0003 µM, showing that **1b** is not only highly photocytotoxic under normoxic conditions, but also under hypoxic conditions as prevalent in the majority of solid tumours[9, 56] that can lead to hypoxic drug resistance[8] especially in the case of PDT agents.[11]

Compound	IC_{50} (irradiation, µM)	IC_{50} (dark, µM)	PI
1a	1.87 ± 0.08	> 2500	> 1300
1b	0.0069 ± 0.0003	> 2500	> 360'000

Tab. 3. The photocytotoxicities and dark toxicities as well as the PIs of **1a** and **1b** in HeLa cells under hypoxic conditions (0.2% O_2, 630 nm, 5.0 J/cm^2).

Mechanism of Action:

In order to determine the cellular uptake pathway of compound **1b**, we inhibited specific uptake pathways in HeLa cells (**S26**). Different uptake pathways were blocked by preincubation with a cationic transporter, metabolic, and endocytotic inhibitors.[54, 57-59] None of the blocked pathways showed an impact on the uptake efficiency of **1b** (**Fig. S18**). Compared to the standard setting, the uptake of **1b** is 26% lower at low temperature (4 °C). This indicates that **1b** is primarily taken up by passive diffusion. Intracellular ROS levels upon irradiation after exposure to **1b** were measured (**S26)**. Compared to **MB** only a minor fraction of the cells tested were ROS-positive after the application of **1b** and subsequent irradiation (**Fig. S19**). This is in line with the observation of low levels of different kinds of ROS generated by **1b** in solution (**Fig. S9**). Together with the observed high photocytotoxicity under hypoxic conditions, these low ROS levels argue that an oxygen-independent MOA is the major cytotoxic pathway. Micrographs visualizing generated intracellular ROS (**Fig. 3b**, **Fig. S20**) were taken (**S28**) and the results are in line with the intracellularly measured ROS levels.

Intracellular localization of **1a** and **1b** was investigated in HeLa cells (**Fig. 3a**, **Fig. S21**) with different dyes for cell organelle staining (**S29**). Both **1a** and **1b** are observable as distinct spherical fluorescent spots and seem to behave similarly after being taken up in the cell. Neither compound co-localized with markers for the nucleus, the mitochondria, the Golgi apparatus, the endoplasmic reticulum, lysosomes or peroxisomes. This indicates that both **1a** and **1b** form local clusters in the cytosol of HeLa cells without specific accumulation in any of the tested cell organelles.

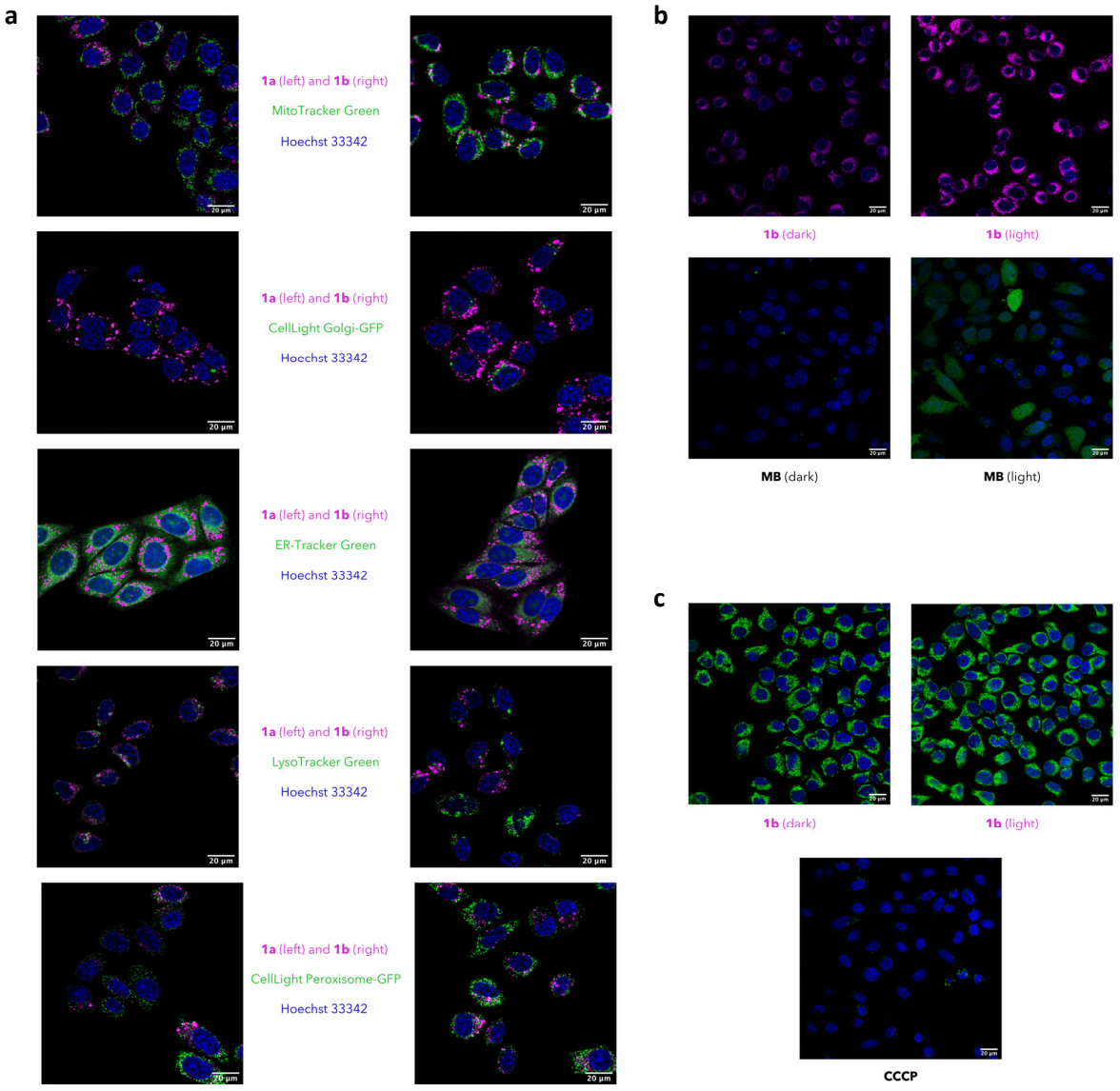

Fig. 3: **a**, Merged intracellular localization images of **1a** and **1b (**shown in purple, $\lambda_{ex/em}$ = 590 / 600-700 nm) in HeLa cells visualised together with the nucleus (shown in blue, Hoechst 33342: $\lambda_{ex/em}$ = 405 / 450-495 nm) and mitochondria (shown in green, MitoTracker Green FM: $\lambda_{ex/em}$ = 488 / 500-550 nm), Golgi apparatus (shown in green, CellLight Golgi-GFP, BacMam 2.0: $\lambda_{ex/em}$ = 488 / 500-550 nm), endoplasmic reticulum (shown in green, ER-Tracker Green: $\lambda_{ex/em}$ = 504 / 514-550 nm), lysosomes (shown in green, LysoTracker Green DND-26: $\lambda_{ex/em}$ = 504 / 514-550 nm), or peroxisomes (shown in green, CellLight Peroxisome-GFP, BacMam 2.0: $\lambda_{ex/em}$ = 488 / 500-550 nm). Images of individual stains are shown in **Fig. S21**. No co-localization with any of the tested organelles is observable for **1a** or **1b**. **b**, Micrographs showing no generated intracellular ROS (shown in green as DCF emission) for **1b** (shown in purple) after irradiation, and intracellular ROS generated by **MB** after irradiation (positive control). The whole set of done experiments is shown in **Fig. S20**. **c**, Micrographs showing no MMP disruption for **1b** after irradiation (emission from the MAK147 dye is shown in green) and MMP disruption induced by **CCCP** (positive control). The whole set of done experiments is shown in **Fig.**

S23.

Next, we tested the ability of **1b** to disrupt the mitochondrial membrane potential (MMP) in HeLa cells (**S30)**. Disruption of the MMP indicates an effect on the mitochondrial electron transfer chain and a failure of mitochondrial function, and is associated with an apoptotic or necrotic cell death mechanism.[60-61] The MMP of HeLa cells was not disrupted after the application of **1b** in the concentration range 0.5 nM – 0.5 µM in the dark, while a clear disruption is visible for **1b** upon application and subsequent irradiation from an applied concentration of 5.0 µM onwards (**Fig. S22**). This concentration is in line with the observed IC_{50} value of **1b** in HeLa cells (**Tab. 2).** Visualization of MMP disruption by **1b** (**Fig. 3c**, **Fig. S23**) was carried out with different concentrations of **1b** in the dark, and upon irradiation (**S31)**. The results were consistent with the MMP disruption experiments.

To investigate the cell death pathway induced by **1b** upon irradiation further, an annexin V/propidium iodide assay in HeLa cells (**Fig. S24**) was applied (**S32)**. This assay shows through changes in the plasma membrane integrity/permeability if cells are viable, apoptotic, or necrotic.[62-63] The observed staining of HeLa cells with the isothiocyanate–annexin V conjugate is in line with the results obtained in the MMP disruption experiment (**Fig. S22**). The cells additionally showed a fluorescent signal upon co-staining with propidium iodide, which indicates a necrotic cell death mechanism since the presence of an intact plasma membrane would prevent propidium iodide from entering early apoptotic cells.[64] To exclude a photoredox-based MOA[23-24] of **1b** in HeLa cells, the intracellular NAD/NADH levels (**Fig. S25**) and GSH/GSSG levels (**Fig. S26**) of HeLa cells treated with **1b** upon irradiation were determined (**S33-S34**). No relevant changes in levels of either NAD/NADH or GSH/GSSG are observed upon treatment with **1b** and subsequent irradiation in the range size of its IC_{50} value. This shows that the MOA of **1b** in HeLa cells is not photoredox-induced.

To investigate the clusters formed by **1a** and **1b** that were observed in the intracellular localization experiments (**Fig. 3a**), dynamic light scattering (DLS) was used (**S35)** to examine whether aggregates of **1a** and **1b** form in the cellular environment (**Tab. S12**). Both **1a** and **1b** form aggregates in DMEM, which was used as a model system to test the aggregation behaviour since it is the most common cell medium for culturing mammalian cells.[65] For **1a** an aggregate size distribution of 122 ± 46 (31.4%), 6 ± 2 (51.3%), and 0.65 ± 0.04 (31.4%) nm was observed, for **1b** a size distribution of 4620 ± 819 (2.0%), 86 ± 33 (79.7%), and 3.8 ± 0.6 (18.3%) nm was observed. Aggregates formed by **1b** in the cell upon irradiation could give rise to a photothermal MOA of **1b** upon irradiation involving a that triggers cell death pathway through the local light-to-heat generation, by the compound clusters similar to nanomaterials applied in PTT.[25] To test this hypothesis, the specific absorption rates (SARs), which are used in literature to experimentally quantify the heating efficiency of compounds[66], of **1a** and **1b** were determined (**Fig. S27**) using a lock-in thermal imaging setup (LIT) measuring the corresponding amplitude (**S36**). Compound **1b** shows overall higher SAR values compared to **1a** (**Tab. 4, Fig. 4**), which is in line with the behaviour of the compounds regarding photocytotoxicity (**Tab. 2**). While the SAR values of **1a** lie in a compound concentration range of 6.25 µM to 100 µM virtually steady slightly

below 2000 W/g, the ones of **1b** show a clear dependency on the concentration ranging from around 16'000 W/g at 100 µM to 6000 W/g at 6.25µM. This shows the SAR of **1b** increases with lower concentrations, most likely due to the higher solvated state of individual molecules, indicating that at compound concentrations present in HeLa cells a photothermal MOA emerging from locally formed clusters of **1b** is conceivable.

Compound	Concentration (µM)	Amplitude A (K) $\times 10^{-3}$	Heating Slope β (K/s) $\times 10^{-2}$	SAR (W/g) $\times 10^{3}$
1a	6.25	0.1 ± 0.1	0.2 ± 0.2	1.7 ± 1.5
1a	12.5	0.3 ± 0.1	0.4 ± 0.2	1.9 ± 0.8
1a	25	0.54 ± 0.07	0.7 ± 0.1	1.6 ± 0.2
1a	50	1.33 ± 0.06	1.7 ± 0.1	1.97 ± 0.09
1a	100	2.5 ± 0.3	3.1 ± 0.4	1.8 ± 0.2
1b	6.25	1.8 ± 0.2	2.3 ± 0.2	16 ± 1
1b	12.5	3.2 ± 0.2	4.0 ± 0.2	14.0 ± 0.8
1b	25	5.8 ± 0.3	7.3 ± 0.3	12.8 ± 0.6
1b	50	8.7 ± 0.1	10.9 ± 0.1	9.6 ± 0.1
1b	100	11.3 ± 0.4	14.2 ± 0.5	6.2 ± 0.2

Tab. 4. The measured amplitude A, heating slope β, and calculated specific absorption rates (SAR) for **1a** and **1b** based on measurements by lock-in thermal imaging (LIT).

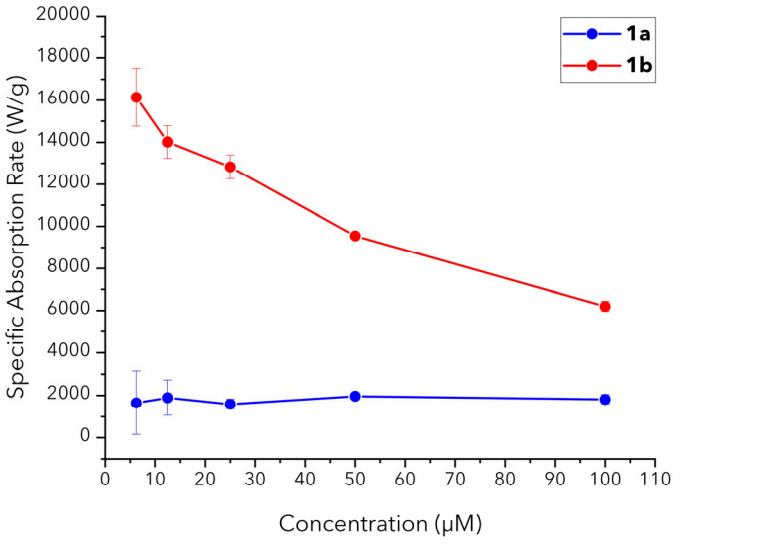

Fig. 4: Specific absorption rates (W/g) of **1a** and **1b** plotted versus the concentration. A clear increase of the SAR values for lower concentrations of **1b** is observed, while the SAR of **1a** virtually shows no concentration dependency.

Discussion:

The presence of molecular oxygen in the tissue to be treated plays a crucial role in the MOA of PDT, making this approach ineffective in tumours surrounded by necrotic tissue or dense tumour masses.[67] Different strategies, such as the application of oxygen vehicles, have been proposed to overcome the barrier posed to PDT by the hypoxic environment in solid tumours.[68] This environment arises from the abnormal structure of the microvessels and tumour microenvironment that leads to ineffective blood distribution,[68] and leads to low oxygen levels that limit PDT.[69] PTT is one photoinduction strategy that would circumvent this limitation, since the therapeutic efficiency of PTT is not affected by oxygen levels.[70] It is even possible that PDT could be combined with PTT to produce a synergistic effect, even in solid tumours.[70-71]

Here we examined small molecules that can act as photothermal agents. With only minute levels of ROS generated upon irradiation, as detected by applied ROS sensors (**Fig. S9**) in PBS as well as intracellularly in HeLa cells (**Figures 3b**, **S19 - S20**), the main MOA of **1a**, **1b**, **2a**, **2b**, **3a**, and **3b** is photothermal (**Tab. 4, Fig. 4**) and bypasses the limitation of PDT. A particularly interesting insight comes from examination of the compound pair **3a** and **3b**. While both compounds show an energetically accessible first excited triplet state (T_1) energy levels based on the results from TDDFT simulations (**Tab. S7**, **Tab. S8**), no $^1O_2$ production was observed (**Tab. 1**), which is in line with the non-existent T_1 state observed in the τ_T measurements (**Tab. 1**). Despite this, both compounds show high photocytotoxicity (**Tab. 2**).

The oxygen-independent MOA of the most effective compound, **1b**, was demonstrated upon irradiation under hypoxia in HeLa cells (**Tab. 3**, **Fig. S17**), where virtually no change in the high effectivity was observed. Additionally, a high efficiency of **1b** in HeLa MCTS was confirmed upon irradiation (**Fig. 2, Tab. S11**, **Fig. S16**), underlining the effectivity of the reported agents. Despite the benefits of the MOA of PTT regarding tumour hypoxia, bio- and nanomaterials applied in PTT show limitations especially concerning biocompatibility, biodegradation and long-term toxicity.[25] Compounds **1a**, **1b**, **2a**, **2b**, **3a**, and **3b** are all small molecules with molecular weights below 600 g/mol, and do not contain any metal atoms. Their non-toxic behaviour in HeLa cells in the dark is indicated by an experimental IC_{50} value up to and > 5 mM. However, upon irradiation these compounds become potent photocytotoxic agents with IC_{50} values as low as 0.0060 ± 0.0003 μM (**Tab. 2**), showing that their molecular character overcomes the biocompatibility problems of materials currently applied in PTT.

Conclusions:

The experiments presented have shown that the reported compounds **1a**, **1b**, **2a**, **2b**, **3a**, and **3b** show multiple advantages over established agents for PDT as well as PTT. The novel compounds are easily accessible synthetically and are all metal-free small molecules. They are virtually non-toxic in the dark, which bypasses the biocompatibility/-degradation and toxicity issues found in the applied materials previously used for PTT. SAR determination experiments demonstrate the light-to-heat generation abilities of these compounds, especially of **1b** which shows particularly high SAR values with low concentrations. The agents are also over 830'000 times more toxic after light activation combined with a photothermal and oxygen-independent MOA (PI of over 360'000 under hypoxic condition of 0.2% O_2), to the best of our knowledge the highest values reported so far (compare with [72]). In short, these compounds show high potential for overcoming the existing drawbacks of PDT and PTT.

Acknowledgements:

We thank the University of Zurich and the R'Equip programme of the Swiss National Science Foundation (project number 206021_164018) for financial support. L.S. was supported by a UZH Forschungskredit grant (Forschungskredit-Beitrag FK-085-19, co-financed together with the Colbianco Stiftung). We kindly thank Prof. Dr. Roland H. Wenger for providing us with the hypoxia facility and Patrick Spielmann for his help in carrying out the hypoxia experiments. We thank Dr. Thomas Fox for assistance with NMR spectroscopy, Dr. Frank Schumer for synthesizing the APF, Dr. Sabbi Lall from Life Science Editors for valuable comments about our manuscript and Dr. Jan Helbing, PD Dr. Stefano Ferrari as well as Prof. Dr. Pablo Rivera-Fuentes for stimulating discussions. Imaging was performed with support and equipment maintained by the Center for Microscopy and Image Analysis, University of Zurich. FACS experiments were performed with support and equipment maintained by the Cytometry Facility, University of Zurich. The authors would like to acknowledge the company NanoLockin for providing the Calorsito device.

Author Contributions:

L.S. designed the compounds and chemical experiments, analysed the corresponding data, coordinated the project, and wrote the paper. M.K. designed and carried out biological experiments and the specific absorption rate determination, and analysed the corresponding data. L.S., S.K., S.S. and V.V. synthesized the compounds and carried out chemical and photophysical experiments as wells the chemical analysis of the synthesized compounds. J.M. carried out the TDDFT simulations and the calculation of the natural transition orbitals. F.K. carried out the fluorescence lifetimes and triplet state lifetime measurements. E.S. and B.S. carried out single crystal X-ray measurements and analysed the data. M.B. provided the Calorsito VIS-NIR device. S.L., C.M., and B.S. were responsible for resources,

supervision, and funding acquisition. All authors discussed the results and commented on the manuscript. All authors approved the final version of the manuscript.

Competing Interests:

M. B. has an equity interest in the company NanoLockin GmbH, that may potentially benefit from the research results.

Data Availability:

Unless mentioned otherwise in the corresponding section, the data that support the findings of this study are available within the paper and its Supplementary Information, or from the corresponding authors on reasonable request. CCDC 2108866–2108875 contain the supplementary crystallographic data for this paper. These data are provided free of charge by The Cambridge Crystallographic Data Centre via www.ccdc.cam.ac.uk/structures.

References:

1. Zhang, J.; Jiang, C.; Figueiró Longo, J. P.; Azevedo, R. B.; Zhang, H.; Muehlmann, L. A., An updated overview on the development of new photosensitizers for anticancer photodynamic therapy. *Acta Pharm. Sin. B* **2018,** *8* (2), 137-146.
2. Lan, M.; Zhao, S.; Liu, W.; Lee, C.-S.; Zhang, W.; Wang, P., Photosensitizers for Photodynamic Therapy. *Adv. Healthcare Mater.* **2019,** *8* (13), 1900132.
3. De Silva, P.; Saad, M. A.; Thomsen, H. C.; Bano, S.; Ashraf, S.; Hasan, T., Photodynamic therapy, priming and optical imaging: Potential co-conspirators in treatment design and optimization — a Thomas Dougherty Award for Excellence in PDT paper. *J. Porphyrins Phthalocyanines* **2020,** *24* (11-12), 1320-1360.
4. van Straten, D.; Mashayekhi, V.; de Bruijn, H. S.; Oliveira, S.; Robinson, D. J., Oncologic Photodynamic Therapy: Basic Principles, Current Clinical Status and Future Directions. *Cancers* **2017,** *9* (2), 19.
5. Agostinis, P.; Berg, K.; Cengel, K. A.; Foster, T. H.; Girotti, A. W.; Gollnick, S. O.; Hahn, S. M.; Hamblin, M. R.; Juzeniene, A.; Kessel, D.; Korbelik, M.; Moan, J.; Mroz, P.; Nowis, D.; Piette, J.; Wilson, B. C.; Golab, J., Photodynamic Therapy of Cancer: An Update. *CA Cancer J. Clin.* **2011,** *61* (4), 250-281.
6. Yanovsky, R. L.; Bartenstein, D. W.; Rogers, G. S.; Isakoff, S. J.; Chen, S. T., Photodynamic therapy for solid tumors: A review of the literature. *Photodermatol. Photoimmunol. Photomed.* **2019,** *35* (5), 295-303.
7. Abrahamse, H.; Hamblin, M. R., New photosensitizers for photodynamic therapy. *Biochem. J.* **2016,** *473*, 347-364.

8. Herman, T. S.; Teicher, B. A.; Collins, L. S., Effect of Hypoxia and Acidosis on the Cytotoxicity of 4 Platinum Complexes at Normal and Hyperthermic Temperatures. *Cancer Res.* **1988,** *48* (9), 2342-2347.
9. Brown, J. M., Tumor Hypoxia in Cancer Therapy. *Methods Enzymol.* **2007,** *435*, 295-321.
10. Baptista, M. S.; Cadet, J.; Di Mascio, P.; Ghogare, A. A.; Greer, A.; Hamblin, M. R.; Lorente, C.; Nunez, S. C.; Ribeiro, M. S.; Thomas, A. H.; Vignoni, M.; Yoshimura, T. M., Type I and Type II Photosensitized Oxidation Reactions: Guidelines and Mechanistic Pathways. *Photochem. Photobiol.* **2017,** *93* (4), 912-919.
11. Pucelik, B.; Sułek, A.; Barzowska, A.; Dąbrowski, J. M., Recent advances in strategies for overcoming hypoxia in photodynamic therapy of cancer. *Cancer Lett.* **2020,** *492*, 116–135.
12. Hong, L.; Li, J.; Luo, Y.; Guo, T.; Zhang, C.; Ou, S.; Long, Y.; Hu, Z., Recent Advances in Strategies for Addressing Hypoxia in Tumor Photodynamic Therapy. *Biomolecules* **2022,** *12* (1), 81.
13. Wilson, B. C.; Patterson, M. S., The physics, biophysics and technology of photodynamic therapy. *Phys. Med. Biol.* **2008,** *53* (9), R61-R109.
14. Gál, D., Effect of photosensitizers in chemical and biological processes: The MTO mechanism in photodynamic therapy. *Biochem. Biophys. Res. Commun.* **1992,** *186* (2), 1032-1036.
15. Vidóczy, T.; Elzemzam, S.; Gál, D., Physico-chemical modeling of the role of free radicals in photodynamic therapy. I. Utilization of quantum yield data of singlet oxygen formation for the study of the interaction between excited photosensitizer and stable free radicals. *Biochem. Biophys. Res. Commun.* **1992,** *189* (3), 1548-1552.
16. Kriska, T.; Jakus, J.; Keszler, A.; Vanyur, R.; Nemeth, A.; Gal, D., Type III photosensitization: attempt for quantification and a way toward new sensitizers. *Proc. SPIE* **1999,** *3563*, 11-17.
17. Gal, D.; Kriska, T.; Shutova, T.; Nemeth, A., Additional approach to PDT: type III mechanism and the role of native free radicals. *Proc. SPIE* **2001,** *4248*, 169-178.
18. Scherer, K. M.; Bisby, R. H.; Botchway, S. W.; Parker, A. W., New Approaches to Photodynamic Therapy from Types I, II and III to Type IV Using One or More Photons. *Anti-Cancer Agents Med. Chem.* **2017,** *17* (2), 171-189.
19. Yoon, I.; Li, J. Z.; Shim, Y. K., Advance in Photosensitizers and Light Delivery for Photodynamic Therapy. *Clin. Endosc.* **2013,** *46* (1), 7-23.
20. Smith, G.; McGimpsey, W. G.; Lynch, M. C.; Kochevar, I. E.; Redmond, R. W., An Efficient Oxygen Independent Two-Photon Photosensitization Mechanism. *Photochemistry and Photobiology* **1994,** *59* (2), 135-139.
21. Dall'Acqua, F.; Martelli, P., Photosensitizing action of furocoumarins on membrane components and consequent intracellular events. *J. Photochem. Photobiol. B* **1991,** *8* (3), 235-254.
22. Hamblin, M. R.; Abrahamse, H., Oxygen-Independent Antimicrobial Photoinactivation: Type III Photochemical Mechanism? *Antibiotics* **2020,** *9* (2), 53.
23. Huang, H. Y.; Banerjee, S.; Qiu, K. Q.; Zhang, P. Y.; Blacque, O.; Malcomson, T.; Paterson, M. J.; Clarkson, G. J.; Staniforth, M.; Stavros, V. G.; Gasser, G.; Chao, H.; Sadler, P. J., Targeted photoredox catalysis in cancer cells. *Nat. Chem.* **2019,** *11* (11), 1041-1048.
24. Li, M.; Gebremedhin, K. H.; Ma, D.; Pu, Z.; Xiong, T.; Xu, Y.; Kim, J. S.; Peng, X., Conditionally Activatable Photoredox Catalysis in Living Systems. *J. Am. Chem. Soc.* **2022,** *144* (1), 163-173.
25. Wei, W.; Zhang, X.; Zhang, S.; Wei, G.; Su, Z., Biomedical and bioactive engineered nanomaterials for targeted tumor photothermal therapy: A review. *Mater. Sci. Eng. C* **2019,** *104*, 109891.
26. Jung, H. S.; Verwilst, P.; Sharma, A.; Shin, J.; Sessler, J. L.; Kim, J. S., Organic molecule-based photothermal agents: an expanding photothermal therapy universe. *Chem. Soc. Rev.* **2018,** *47* (7), 2280-2297.

27. Anand, S.; Chan, T. A.; Hasan, T.; Maytin, E. V., Current Prospects for Treatment of Solid Tumors via Photodynamic, Photothermal, or Ionizing Radiation Therapies Combined with Immune Checkpoint Inhibition (A Review). *Pharmaceuticals* **2021,** *14* (5), 447.

28. Su, M.; Han, Q.; Yan, X.; Liu, Y.; Luo, P.; Zhai, W.; Zhang, Q.; Li, L.; Li, C., A Supramolecular Strategy to Engineering a Non-photobleaching and Near-Infrared Absorbing Nano-J-Aggregate for Efficient Photothermal Therapy. *ACS Nano* **2021,** *15* (3), 5032-5042.

29. He, Z.; Zhao, L.; Zhang, Q.; Chang, M.; Li, C.; Zhang, H.; Lu, Y.; Chen, Y., An Acceptor–Donor–Acceptor Structured Small Molecule for Effective NIR Triggered Dual Phototherapy of Cancer. *Adv. Funct. Mater.* **2020,** *30* (16), 1910301.

30. Li, X.; Fang, F.; Sun, B.; Yin, C.; Tan, J.; Wan, Y.; Zhang, J.; Sun, P.; Fan, Q.; Wang, P.; Li, S.; Lee, C.-S., Near-infrared small molecule coupled with rigidness and flexibility for high-performance multimodal imaging-guided photodynamic and photothermal synergistic therapy. *Nanoscale Horiz.* **2021,** *6* (2), 177-185.

31. Huang, S.; Kannadorai, R. K.; Chen, Y.; Liu, Q.; Wang, M., A narrow-bandgap benzobisthiadiazole derivative with high near-infrared photothermal conversion efficiency and robust photostability for cancer therapy. *Chem. Commun.* **2015,** *51* (20), 4223-4226.

32. Naik, A.; Rubbiani, R.; Gasser, G.; Spingler, B., Visible-Light-Induced Annihilation of Tumor Cells with Platinum–Porphyrin Conjugates. *Angew. Chem. Int. Ed.* **2014,** *53* (27), 6938-6941.

33. Antoni, P. M.; Naik, A.; Albert, I.; Rubbiani, R.; Gupta, S.; Ruiz-Sanchez, P.; Munikorn, P.; Mateos, J. M.; Luginbuehl, V.; Thamyongkit, P.; Ziegler, U.; Gasser, G.; Jeschke, G.; Spingler, B., (Metallo)porphyrins as Potent Phototoxic Anti-Cancer Agents after Irradiation with Red Light. *Chem. Eur. J.* **2015,** *21* (3), 1179-1183.

34. Wu Klingler, W.; Giger, N.; Schneider, L.; Babu, V.; König, C.; Spielmann, P.; Wenger, R. H.; Ferrari, S.; Spingler, B., Low-Dose Near-Infrared Light-Activated Mitochondria-Targeting Photosensitizers for PDT Cancer Therapy. *Int. J. Mol. Sci.* **2022,** *23* (17), 9525.

35. Hao, E.; Xu, Y.; Yu, C.; Jiao, L. Near-infrared 4-difluoro-4-borata-3a-azonia-4a-aza-s-indacene fluorescent dye and preparation method thereof. CN103952001B, 2014.

36. Padrutt, R.; Babu, V.; Klingler, S.; Kalt, M.; Schumer, F.; Anania, M. I.; Schneider, L.; Spingler, B., Distyryl-BODIPY-Transplatin Conjugates as Highly Phototoxic Photosensitizers for Photodynamic Therapy. *ChemMedChem* **2021,** *16* (4), 694-701.

37. Xiao, Y.-F.; Chen, J.-X.; Chen, W.-C.; Zheng, X.; Cao, C.; Tan, J.; Cui, X.; Yuan, Z.; Ji, S.; Lu, G.; Liu, W.; Wang, P.; Li, S.; Lee, C.-S., Achieving high singlet-oxygen generation by applying the heavy-atom effect to thermally activated delayed fluorescent materials. *Chem. Commun.* **2021,** *57* (40), 4902-4905.

38. Jiang, X.-J.; Lau, J. T. F.; Wang, Q.; Ng, D. K. P.; Lo, P.-C., pH- and Thiol-Responsive BODIPY-Based Photosensitizers for Targeted Photodynamic Therapy. *Chem. Eur. J.* **2016,** *22* (24), 8273-8281.

39. Schneider, L.; Larocca, M.; Wu, W.; Babu, V.; Padrutt, R.; Slyshkina, E.; König, C.; Ferrari, S.; Spingler, B., Exocyclically metallated tetrapyridinoporphyrazine as a potential photosensitizer for photodynamic therapy. *Photochem. Photobiol. Sci.* **2019,** *18* (11), 2792-2803.

40. Rubbiani, R.; Wu, W.; Naik, A.; Larocca, M.; Schneider, L.; Padrutt, R.; Babu, V.; König, C.; Hinger, D.; Maake, C.; Ferrari, S.; Gasser, G.; Spingler, B., Studying the cellular distribution of highly phototoxic platinated metalloporphyrins by isotope labelling. *Chem. Commun.* **2020,** *56* (92), 14373-14376.

41. Le, N. A.; Babu, V.; Kalt, M.; Schneider, L.; Schumer, F.; Spingler, B., Photo-stable platinated bacteriochlorins as potent photodynamic agents. *J. Med. Chem.* **2021,** *64* (10), 6792–6801.

42. Schneider, L.; Kalt, M.; Larocca, M.; Babu, V.; Spingler, B., Potent PBS-Soluble Transplatin Derived Porphyrin-Based Photosensitizer for Photodynamic Therapy. *Inorg. Chem.* **2021,** *60* (13), 9416–9426.

43. Rurack, K.; Kollmannsberger, M.; Daub, J., Molecular Switching in the Near Infrared (NIR) with a Functionalized Boron–Dipyrromethene Dye. *Angew. Chem. Int. Ed.* **2001,** *40* (2), 385-387.

44. Baruah, M.; Qin, W.; Flors, C.; Hofkens, J.; Vallée, R. A. L.; Beljonne, D.; Van der Auweraer, M.; De Borggraeve, W. M.; Boens, N., Solvent and pH dependent fluorescent properties of a dimethylaminostyryl borondipyrromethene dye in solution. *J. Phys. Chem. A* **2006,** *110* (18), 5998-6009.

45. Deniz, E.; Isbasar, G. C.; Bozdemir, Ö. A.; Yildirim, L. T.; Siemiarczuk, A.; Akkaya, E. U., Bidirectional Switching of Near IR Emitting Boradiazaindacene Fluorophores. *Org. Lett.* **2008,** *10* (16), 3401-3403.

46. Pucelik, B.; Paczynski, R.; Dubin, G.; Pereira, M. M.; Arnaut, L. G.; Dabrowski, J. M., Properties of halogenated and sulfonated porphyrins relevant for the selection of photosensitizers in anticancer and antimicrobial therapies. *PLoS One* **2017,** *12* (10), e0185984.

47. Becke, A. D., Density-functional exchange-energy approximation with correct asymptotic behavior. *Phys. Rev. A* **1988,** *38* (6), 3098-3100.

48. Lee, C.; Yang, W.; Parr, R. G., Development of the Colle-Salvetti correlation-energy formula into a functional of the electron density. *Phys. Rev. B* **1988,** *37* (2), 785-789.

49. Becke, A. D., Density-functional thermochemistry. III. The role of exact exchange. *J. Chem. Phys.* **1993,** *98* (7), 5648-5652.

50. Stephens, P. J.; Devlin, F. J.; Chabalowski, C. F.; Frisch, M. J., Ab Initio Calculation of Vibrational Absorption and Circular Dichroism Spectra Using Density Functional Force Fields. *J. Chem. Phys.* **1994,** *98* (45), 11623-11627.

51. Martin, R. L., Natural transition orbitals. *J. Chem. Phys.* **2003,** *118* (11), 4775-4777.

52. Klamt, A.; Schüürmann, G., COSMO: a new approach to dielectric screening in solvents with explicit expressions for the screening energy and its gradient. *J. Chem. Soc., Perkin Trans. 2* **1993,** (5), 799-805.

53. Zorlu, Y.; Dumoulin, F.; Durmuş, M.; Ahsen, V., Comparative studies of photophysical and photochemical properties of solketal substituted platinum(II) and zinc(II) phthalocyanine sets. *Tetrahedron* **2010,** *66* (17), 3248-3258.

54. Karges, J.; Kuang, S.; Maschietto, F.; Blacque, O.; Ciofini, I.; Chao, H.; Gasser, G., Rationally designed ruthenium complexes for 1- and 2-photon photodynamic therapy. *Nat. Commun.* **2020,** *11*, 3262.

55. Friedrich, J.; Seidel, C.; Ebner, R.; Kunz-Schughart, L. A., Spheroid-based drug screen: considerations and practical approach. *Nat. Prot.* **2009,** *4* (3), 309-324.

56. Muz, B.; de la Puente, P.; Azab, F.; Azab, A. K., The role of hypoxia in cancer progression, angiogenesis, metastasis, and resistance to therapy. *Hypoxia* **2015,** *3*, 83-92.

57. Li, C.; Yu, M.; Sun, Y.; Wu, Y.; Huang, C.; Li, F., A Nonemissive Iridium(III) Complex That Specifically Lights-Up the Nuclei of Living Cells. *J. Am. Chem. Soc.* **2011,** *133* (29), 11231-11239.

58. Lazarenko, R. M.; DelBove, C. E.; Strothman, C. E.; Zhang, Q., Ammonium chloride alters neuronal excitability and synaptic vesicle release. *Sci. Rep.* **2017,** *7* (1), 5061.

59. Harper, J. N.; Wright, S. H., Multiple mechanisms of ligand interaction with the human organic cation transporter, OCT2. *Amer. J. Physiol. Renal Phys.* **2012,** *304* (1), F56-F67.

60. Ricci, J.-E.; Muñoz-Pinedo, C.; Fitzgerald, P.; Bailly-Maitre, B.; Perkins, G. A.; Yadava, N.; Scheffler, I. E.; Ellisman, M. H.; Green, D. R., Disruption of Mitochondrial Function during Apoptosis Is Mediated by Caspase Cleavage of the p75 Subunit of Complex I of the Electron Transport Chain. *Cell* **2004,** *117* (6), 773-786.

61. Skulachev, V. P., Bioenergetic aspects of apoptosis, necrosis and mitoptosis. *Apoptosis* **2006,** *11* (4), 473-485.

62. Vermes, I.; Haanen, C.; Steffens-Nakken, H.; Reutellingsperger, C., A novel assay for apoptosis Flow cytometric detection of phosphatidylserine expression on early apoptotic cells using fluorescein labelled Annexin V. *J. Immunol. Methods* **1995,** *184* (1), 39-51.

63. Vermes, I.; Haanen, C.; Reutelingsperger, C., Flow cytometry of apoptotic cell death. *J. Immunol. Methods* **2000,** *243* (1), 167-190.

64. Darzynkiewicz, Z.; Bruno, S.; Del Bino, G.; Gorczyca, W.; Hotz, M. A.; Lassota, P.; Traganos, F., Features of apoptotic cells measured by flow cytometry. *Cytometry* **1992,** *13* (8), 795-808.

65. Hemelaar, S. R.; Nagl, A.; Bigot, F.; Rodríguez-García, M. M.; de Vries, M. P.; Chipaux, M.; Schirhagl, R., The interaction of fluorescent nanodiamond probes with cellular media. *Microchim. Acta* **2017,** *184* (4), 1001-1009.

66. Steinmetz, L.; Kirsch, C.; Geers, C.; Petri-Fink, A.; Bonmarin, M., Investigating a Lock-In Thermal Imaging Setup for the Detection and Characterization of Magnetic Nanoparticles. *Nanomaterials* **2020,** *10* (9), 1665.

67. Calixto, G. M. F.; Bernegossi, J.; de Freitas, L. M.; Fontana, C. R.; Chorilli, M., Nanotechnology-Based Drug Delivery Systems for Photodynamic Therapy of Cancer: A Review. *Molecules* **2016,** *21* (3), 342.

68. Larue, L.; Myrzakhmetov, B.; Ben-Mihoub, A.; Moussaron, A.; Thomas, N.; Arnoux, P.; Baros, F.; Vanderesse, R.; Acherar, S.; Frochot, C., Fighting Hypoxia to Improve PDT. *Pharmaceuticals* **2019,** *12* (4), 163.

69. Gunaydin, G.; Gedik, M. E.; Ayan, S., Photodynamic Therapy—Current Limitations and Novel Approaches. *Front. Chem.* **2021,** *9*, 691697.

70. Bian, W.; Wang, Y.; Pan, Z.; Chen, N.; Li, X.; Wong, W.-L.; Liu, X.; He, Y.; Zhang, K.; Lu, Y.-J., Review of Functionalized Nanomaterials for Photothermal Therapy of Cancers. *ACS Appl. Nano Mater.* **2021,** *4* (11), 11353-11385.

71. Tian, B.; Wang, C.; Zhang, S.; Feng, L.; Liu, Z., Photothermally Enhanced Photodynamic Therapy Delivered by Nano-Graphene Oxide. *ACS Nano* **2011,** *5* (9), 7000-7009.

72. Cole, H. D.; Roque, J. A.; Shi, G.; Lifshits, L. M.; Ramasamy, E.; Barrett, P. C.; Hodges, R. O.; Cameron, C. G.; McFarland, S. A., Anticancer Agent with Inexplicable Potency in Extreme Hypoxia: Characterizing a Light-Triggered Ruthenium Ubertoxin. *J. Am. Chem. Soc.* **2022,** *144* (22), 9543–9547.

ToC

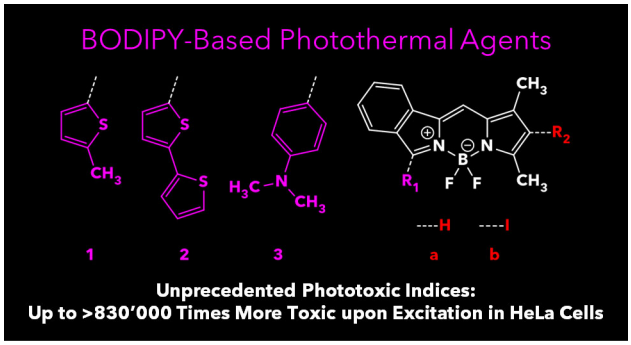
BODIPY-Based Photothermal Agents
S
CH3
S
S
H3C
N
CH3
CH3
R2
N
B
N
R1
F
F
CH3
----H
----I
1
2
3
a
b
Unprecedented Phototoxic Indices:
Up to >830'000 Times More Toxic upon Excitation in HeLa Cells